Article

Utilization of *Azadirachta indica* Sawdust as a Potential Adsorbent for the Removal of Crystal Violet Dye

Zeeshan Ahamad and Abu Nasar *

Department of Applied Chemistry, Faculty of Engineering and Technology, Aligarh Muslim University, Aligarh 202002, India
* Correspondence: abunasaramu@gmail.com; Tel.: +91-0571-2700920 (ext. 3000); Fax: +91-0571-2700528

Abstract: The current study examines the feasibility of recycling artificially polluted wastewater that contains crystal violet (CV) organic dye by using *Azadirachta indica* sawdust (AISD) waste as a highly cost-effective adsorbent. Different analytical techniques, viz., SEM/EDX, TEM/SAED, BET, XRD, TGA-DTG, point of zero charge (pH_{pzc}), and FTIR, were used to characterize the adsorbent. Studies of batch adsorption were performed with varying contact times, starting concentrations of CV, pH levels, doses and particle sizes of AISD, and temperatures. After assessing the results using the Langmuir, Freundlich, and Temkin isotherm models, it was observed that the Langmuir model best fits the data. Various models were employed to analyze the kinetic findings, and it was confirmed that the pseudo-second-order model appears to be the most accurate. The values of $\Delta H°$ (50.01 kJ mol^{-1}), $\Delta G°$ (-10.254 to -5.043 kJ mol^{-1}), and $\Delta S°$ (182.47 J K^{-1}mol^{-1}), obtained in a temperature range of 303–333 K, revealed that the process was spontaneous, endothermic, and accompanied by an increase in entropy. Based on experimental findings and their analyses, it was concluded that the adsorbent made from AISD is one of the most effective among those obtained from domestic, agricultural, and industrial wastes. Thus, the present adsorbent can be effectively exploited to make dye-contaminated water reusable.

Keywords: *Azadirachta indica* sawdust; crystal violet; adsorptive removal; wastewater

1. Introduction

Water free from contamination and toxicity is necessary for human health and well-being, the maintenance of ecosystems, and the growth of the economy [1,2]. The rapid decline in water quality due to pollutants such as heavy metals, dyes, pesticides, and other undesirable substances and the ongoing reduction in freshwater availability are serious issues that cause significant reasons for worry. Declining water quality is also linked with various illnesses and other adverse effects on human health [2–5]. Dyes are the only pollutant that can be seen with the naked eye, even at very low concentrations, making them unique among other contaminants. The effects of dyes may be either acute or chronic, based on the nature, concentration, and duration of dye exposure. Dyes are known to induce a variety of adverse health effects, including, but not limited to skin irritation, respiratory ailments, mental disorders, and vomiting. In many instances, they are also known to be carcinogenic and mutagenic [6–8]. Numerous sectors, such as the rubber, plastics, cosmetics, textile, food, leather, pharmaceutical, photographic processing, wood preservative chemical, pulp and paper, and petroleum industries, employ dyes in their processes [9–11]. The dye market is crowded with a lot of dyes, with over 7×10^5 tonnes of annual production [12]. Most dyes have high photo-stability and thermal stability, and removing them from an aqueous system is difficult because of their stable structure, non-biodegradability, and synthetic origin [13,14]. The dye-based industries release effluents that have not been treated or have only been partially treated, thus posing a significant risk to the local flora and animals [15]. The reduction in the amount of light that can penetrate

the water due to dyes is one of the most significant environmental concerns associated with their use. This negatively affects the ability of aquatic life to engage in photosynthesis, which, in turn, leads to oxygen deficiency [16]. Crystal violet (CV) is a synthetic dye with a dark purple color. It is used in manufacturing veterinary medication, paint, printing ink, etc. It has been reported that this dye is harmful and persists in the environment for a very long period [17]. In addition to this, it inhibits the growth of bacteria and fungi.

The removal of toxic pollutants from an aqueous medium has been accomplished using various methods, including membrane filtration [18–21], ion exchange [22,23], photochemical [24,25], electrodialysis [26–29], coagulation and flocculation [10,30], photocatalysis [31,32], nanofiltration [33,34], electroflotation [35–37], manganese dioxide oxidation [38–40], reverse osmosis [41–44], ozonation [45–47], electrochemical [48,49], etc. For the detoxification of dye-loaded effluents, it has been noted that adsorption is the most appealing of these approaches. This technique is simple, effective, environmentally benign, and cost-effective. However, selecting an appropriate adsorbent has always been a complex problem. Typical adsorbents such as activated carbon and silica gel should be the first options. Still, their use is limited owing to the expensive cost of these materials and the difficulties associated with recycling. In this context, the adsorbents from natural materials mainly obtained from agricultural and domestic wastes have received considerable attention [27,50–52].

Natural materials, widely available as wastes from agricultural operations, are environmentally friendly and could potentially be used to remove dyes from an aqueous medium. Likewise, the sawdust [53] and leaf powder [54] of the neem tree (species: *Azadirachta indica*) have successfully been used as adsorbents for the removal of malachite green and methylene blue, respectively. Due to its abundance in India, it could be exploited as a prospective and inexpensive adsorbent for the easy treatment of dye-laden water. The present study deals with the adsorption potential of *Azadirachta indica* sawdust (AISD) for the removal of CV from aqueous systems.

The present research was planned with a prima facie to utilize AISD adsorbent to purify wastewater effectively. A technique for evaluating complete operational parameters was developed, and AISD was employed for CV dye sequestration. The physicochemical parameters (such as pH, amount of adsorbent, contact time, temperature (T), and various dye concentrations at the starting stage) were optimized. Thermodynamic, isothermal, and kinetic investigations were also carried out along with routine characterizations, namely, SEM/EDXS, TEM/SAED, BET, TGA-DTG, XRD, point of zero charge (pH_{pzc}), and FTIR.

2. Experimental Procedure

2.1. Materials

The CV dye of a biological stain grade procured from Fisher Scientific, Mumbai, India was used as received. In the current experiment, the following analytical reagent-grade chemicals and reagents were utilized: HCl (Fisher Scientific, Mumbai, India), CH_3COOH (SD Fine Chem, Mumbai, India), NaOH (Merck, Darmstadt, Germany), and KNO_3 (CDH, New Delhi, India). A CV stock solution with a concentration of 1000 mg L^{-1} was produced by dissolving the required quantity of CV in water obtained through the double distillation of deionized water (DDDW).

2.2. Adsorbent Preparation

AISD obtained from the local timber was thoroughly cleaned with DDDW to eliminate debris, filth, and other surface impurities. The cleaned mass was dried for about 2 days in sunlight, beneath a white cotton sheet (with an air gap of at least 4 cm between the mass and sheet), and then, for 20 h in an oven at 80 °C. The dry mass was ground into a powder using a motor-driven grinder and extensively washed with DDDW before filtering through an 80 BSS mesh standard sieve. This sieved powder (80 BSS mesh) was again dried for about 2 h in the oven at 80 °C. The raw material mass was then ground into a powder using an agate mortar and pestle. The powder was then stored in airtight containers.

2.3. Adsorbent Characterization

The point of zero charge (pH_{pzc}) of AISD was determined using the solid addition technique, in which 25 mL of 0.1 M KNO_3 was added to several 250 mL conical flasks. Through the drop-by-drop addition of 0.1 M HCl/NaOH to solutions, the initial pH (pH_i) was adjusted from 2 to 13. After adding 0.05 g adsorbent to each beaker, they were adequately covered and left for 48 h in a dark place. After measuring the final pH (pH_f) of each reaction mixture, the point of zero charge was determined from ΔpH (pH_f–pH_i) vs. pH_i plot, as the intersection point on pH_i axis represents the value of pH_{pzc} [55].

A scanning electron microscopy (SEM)/energy dispersive X-ray (EDXS) analyzer (JSM-6510LV, JEOL, Tokyo, Japan) was utilized to investigate the morphologic and elemental characteristics of AISD. Transmission electron microscopy (JEM 2100, JEOL, Tokyo, Japan) was used to examine the size of the adsorbent particles. A surface area analyzer (Smart Sorb 93) was employed to determine the pore volume and surface area of AISD utilizing the Brunauer, Emmett, and Teller (BET) method. X-ray Powder Diffraction (XRD, SmartLab, Rigaku, Japan) was used to investigate the crystallinity or amorphous nature of the adsorbents. The experiments were carried out in a 5°–80° (2θ) range at a 20° min^{-1} scan rate with a 0.02° step size. FTIR (Fourier Transform Infrared Spectrometry) (1800 IR spectrophotometer, Perkin-Elmer, Waltham, MA, USA) was used to analyze the functional groups of the adsorbents (AISD) in a spectral range of 4000–400 cm^{-1} on a KBr pellet. Thermogravimetric analysis (TGA) was performed in a nitrogen environment using a thermogravimetric analyzer (Perkin Elmer, Pyris). A heating rate of 20 °C min^{-1} was maintained in a temperature range of 24 to 750 °C.

2.4. Study of Operational Parameters

Batch adsorption was utilized to optimize the efficacy of AISD in removing CV from synthetically contaminated water. All experiments were performed in 100 mL beakers containing 25 mL dye solution and 0.01 g AISD unless otherwise specified. The batch experiments were conducted after ensuring the pH of the medium was at 7. The peak wavelength (λ_{max}) on a UV-VIS spectrophotometer was adjusted to 588 nm to evaluate the residual concentration of CV in the supernatant collected after adsorption. The equilibrium adsorption capacity (q_e) and the removal efficiency (%R) were determined using the following equations:

$$q_e = (C_o - C_e) \times \frac{V}{M} \tag{1}$$

$$\%R = \frac{(C_o - C_t)}{C_o} \times 100 \tag{2}$$

In the above equations, C_o, C_e, and C_t are the starting, equilibrium, and any time concentration (mg L^{-1}), V is the volume (L) of CV taken, and M (g) is the weight of AISD, respectively. A formula similar to Equation (1) was used to compute the adsorption capacity (q_t) at any time (t).

2.5. Regeneration and Desorption Experiment

A desorption study was performed using a range of desorbing agents including HCl, NaOH, CH_3COOH, NaCl, and DDDW. CV-loaded AISD was extensively cleaned with DDDW to remove the unadsorbed dye. Afterward, 25 mL of each desorbing agent was used to agitate the CV-loaded AISD for 4 h. After desorption, the concentration of CV was determined spectrophotometrically, and desorption was computed using the following equation:

$$\% \, Desorption = \frac{m_d}{m_a} \times 100 \tag{3}$$

Here, m_d and m_a represent the amount of CV desorbed and adsorbed in mg L^{-1}.

3. Results and Discussion

3.1. SEM/EDXS Analyses

Figure 1a,b show the SEM micrographs (1500×) of AISD and CV/AISD. Upon CV adsorption, the variations in the exterior of the adsorbent are reflected in Figure 1b. The porosity and uneven surface of AISD, as seen in the SEM micrographs, offer a suitable place for the adsorption of CV molecules. A significant change in the elemental composition, as shown in Figure 1c,d (EDXS), is observed, including the inclusion of Cl, which points out the adsorption of CV ($C_{25}N_3H_{30}Cl$).
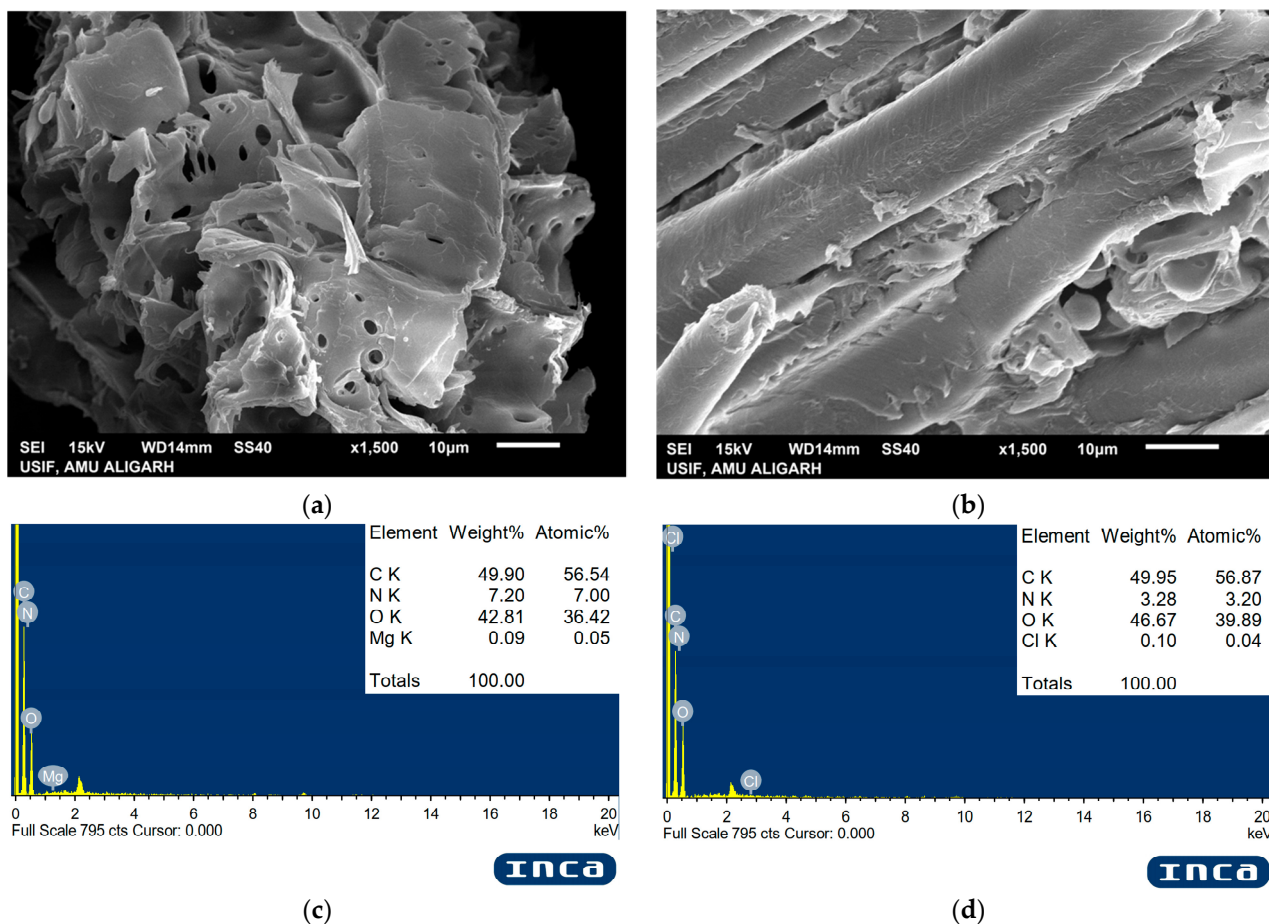

(**a**)

(**b**)

Element	Weight%	Atomic%
C K	49.90	56.54
N K	7.20	7.00
O K	42.81	36.42
Mg K	0.09	0.05
Totals	100.00	

Element	Weight%	Atomic%
C K	49.95	56.87
N K	3.28	3.20
O K	46.67	39.89
Cl K	0.10	0.04
Totals	100.00	

(**c**)

(**d**)

Figure 1. SEM micrographs (1500×) and EDXS outcomes of AISD adsorbent: before adsorption (**a**,**c**) and after adsorption (**b**,**d**).

3.2. TEM Analysis

The TEM image shown in Figure 2a proves the presence of nano-sized particles of AISD ranging from 12 to 42 nm. The nano-ranged particle offers an appropriate surface area to adsorb dye molecules. The SAED pattern (Figure 2b) points out the amorphous nature of the adsorbent, which is further confirmed by the poor crystallinity observed in the XRD studies, which will be discussed in Section 3.4.
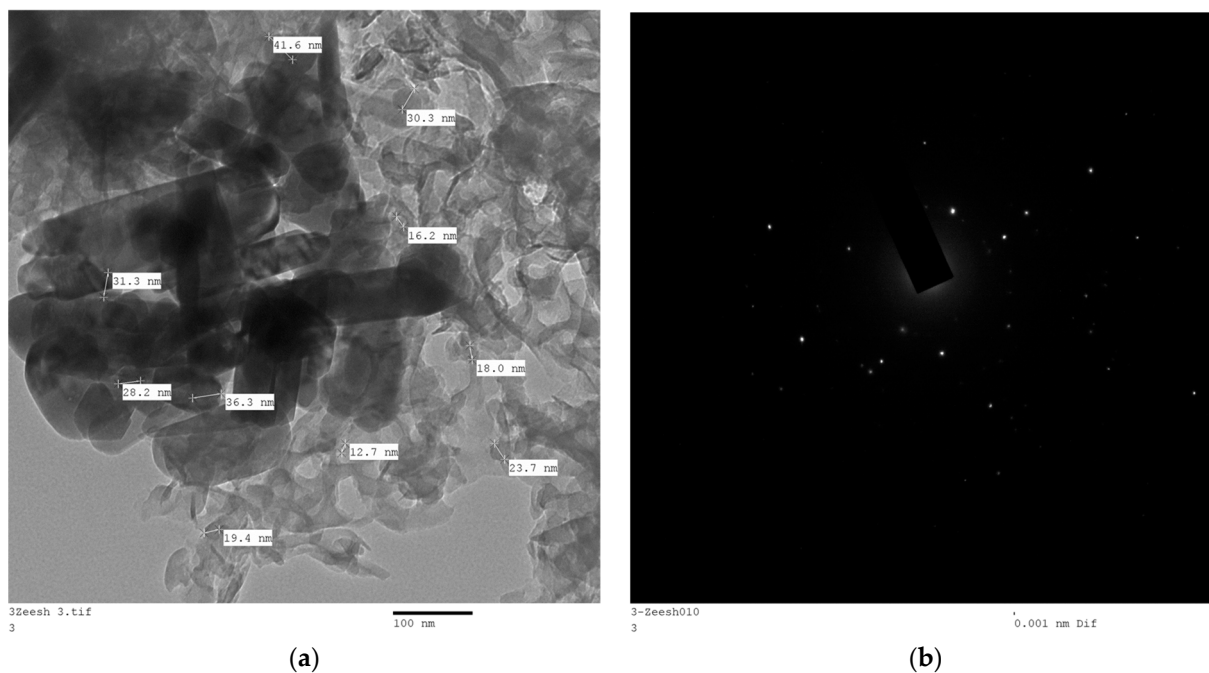
Figure 2. (**a**) TEM image and (**b**) SAED image of AISD.

3.3. BET Analysis

Nitrogen adsorption/desorption analysis was performed in liquid nitrogen at 77 K to find the surface area and pore parameters of AISD. Figure 3a describes the type IV isotherm of H3 hysteresis with a monolayer followed by multilayered capillary condensation [56,57], indicating mesopores in AISD. A multipoint BET equation in a relative pressure range (P P_0^{-1}) of 0.05 to 0.25 (Figure 3b) confirms the surface area of 2.507 m^2 g^{-1}. The Barrett–Joyner–Halenda (BJH) method calculated the corresponding pore size distributions, showing that the material exhibits a 7.78 nm pores size (Figure 3a inset).
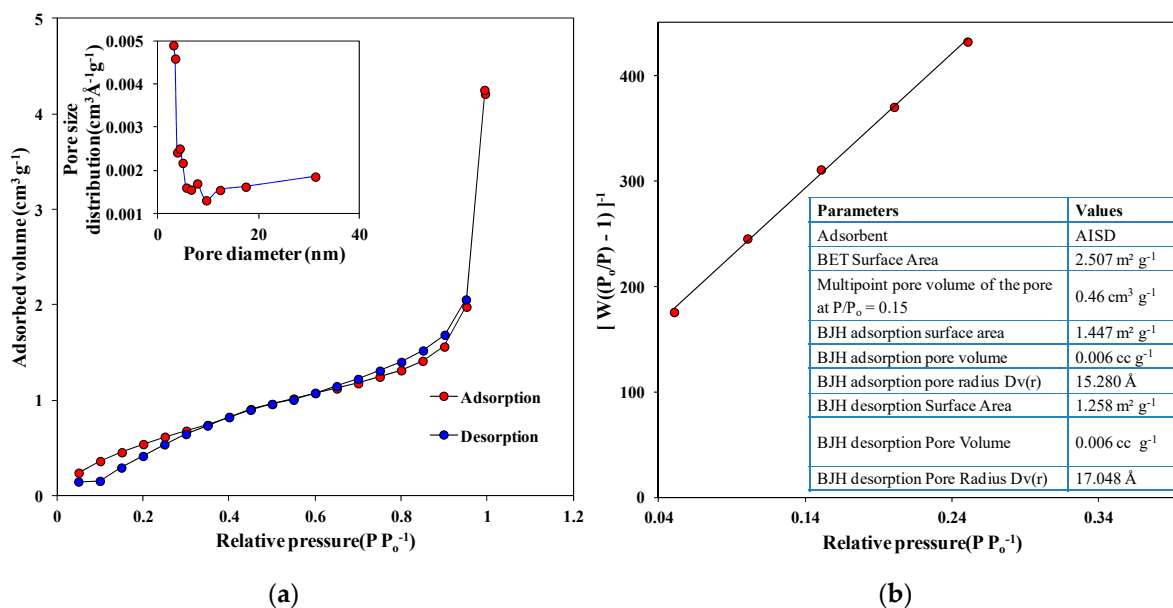

Parameters	Values
Adsorbent	AISD
BET Surface Area	2.507 m^2 g^{-1}
Multipoint pore volume of the pore at P/P_o = 0.15	0.46 cm^3 g^{-1}
BJH adsorption surface area	1.447 m^2 g^{-1}
BJH adsorption pore volume	0.006 cc g^{-1}
BJH adsorption pore radius Dv(r)	15.280 Å
BJH desorption Surface Area	1.258 m^2 g^{-1}
BJH desorption Pore Volume	0.006 cc g^{-1}
BJH desorption Pore Radius Dv(r)	17.048 Å

Figure 3. (**a**) BET nitrogen adsorption-desorption isotherm (inset—BJH pore size distribution vs. pore diameter plot) for AISD and (**b**) multipoint BET plot for AISD.

3.4. XRD Analysis

The XRD patterns (2θ: 5°–80°) shown in Figure 4 (upper inset) indicate that the present adsorbent is a low-crystalline material. The presence of hemicelluloses and lignin is the leading cause of the amorphous nature, as reflected in the XRD pattern of AISD [58]. However, the available crystalline areas of cellulose in AISD are responsible for three peaks in the 2θ range at 16.48°, 22.36°, and 34.54° for AISD. In this context, it is worth mentioning that other investigators have also reported prominent peaks at around 16° and 22° for similar adsorbents such as rubber wood sawdust [59], pinewood [60], *Pinus elliotii* (slash pine) [61], and *Tectona grandis* sawdust [62].
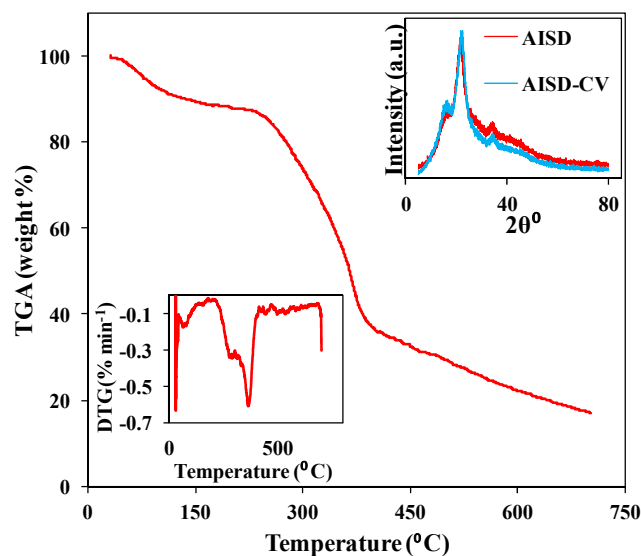

Figure 4. TGA plot of AISD (upper inset—XRD pattern, and lower inset—DTG plot).

3.5. TGA-DTG Analysis

The TGA thermogram of the present adsorbent, shown in Figure 4, indicates that the thermal properties are comparable to those obtained for similar sawdust-based adsorbents, namely, *Terminalia arjuna* [63]. The obtained thermogram can be represented by the various stages of thermal degradation [63]. The initial stage is associated with moisture evaporation. The maximum weight loss in the latter stage is due to the thermal degradation of the most unstable component, hemicellulose. This is followed by the pyrolysis of cellulose. The most stable component, lignin, was last to degrade. In fact, in the case of lignin, breakdown began at room temperature and proceeded up to the entire temperature range [64].

The DTG thermogram of the adsorbent shown in Figure 4 (lower inset) clearly shows the maximum occurring at 354.02 °C, indicating the highest degradation at this temperature.

3.6. FTIR Analysis

The FTIR spectra obtained for loaded and unloaded AISD were used to better understand the availability of distinct functional groups present on the surface of AISD, which are responsible for various types of interactions resulting in the adsorption of CV dye onto AISD. Figure 5 represents the overlapping FTIR spectra of AISD before and after CV dye adsorption. The pristine AISD spectra indicate a strong wideband at 3400 cm^{-1} pertaining to the –OH stretching mode and peaks at 2917 and 2846 cm^{-1} corresponding to the –CH stretching of the alkyl group. The peaks found at 1732, 1619, and 1421 cm^{-1} represent the carbonyl group (C=O stretching vibration), alkene (C=C stretching), amine (–NH bending), alcohol (O–H bending), and alkyl group (C–H bending). Additionally, weak-to-moderate bands in the region of 1232 to 1019 cm^{-1} occur because of the vibration of an alkyl group (–CH$_3$) and of aliphatic 2° amines (C–N stretching), while the band at 882 cm^{-1} is due to the C–H (aromatic) group (Figure 5). The shifting of the band position from 3400, 2917,

2846, 1732, 1619, 1421, 1232, 1136, 1080, 1019, 882, 577, and 428 cm^{-1} to 3412, 2914, 1600, 1457, 1373, 1325, 1222, 1138, 1023, 886 and 636, and 584 cm^{-1} after adsorption point out the adsorptive participation of the respective functional groups present in AISD.
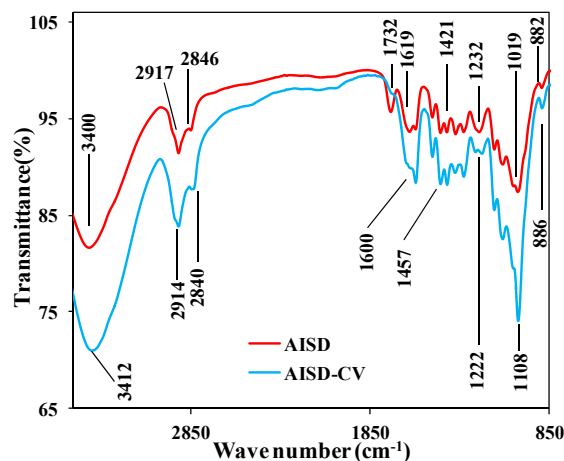

Figure 5. FTIR spectra of AISD and AISD–CV.

3.7. Study of Operational Parameters

3.7.1. Adsorbent Dose

The adsorbent dosage occupies a significant position since it controls adsorption performance, which, in turn, helps to eliminate specific dyes. The effect of the adsorbent dose ranging from 0.4 to 4.0 g L^{-1} on removal efficiency (%R) and adsorption capacity is shown (Figure 6 inset) under the chosen experimental conditions of C$_o$ = 100 mg L^{-1}, contact time = 90 min, pH = 7.0, and temperature = 303 K. At equilibrium, the %R improves from 58.32 to 93.36 %, when the adsorbent dosage is increased from 0.4 to 4.0 g L^{-1}. The rise in %R is due to the increasing availability of binding sites at the higher dose. However, as seen in the figure, an opposite trend in adsorption efficiency, i.e., a decrease in adsorption capacity with increasing dose, is observed. This is attributed to the decline in adsorption sites per unit weight of adsorbents at the higher dose. In fact, at higher doses, adsorbent molecules associate and agglomerate, resulting in a reduction in surface area per unit mass of the adsorbent [55]. Therefore, the optimum dose of 0.4 g L^{-1} was judiciously chosen for further experiments.

3.7.2. Initial Dye Concentration (C$_o$) and Contact Time

At 303 K, at varied starting dye concentrations of CV of 25, 50, 75, and 100 mg L^{-1}, the impact on CV adsorption ability onto AISD was investigated. The findings are plotted in Figure 6. The data demonstrate that the initial 20 min show a significant rise in the adsorption capacity of CV onto the AISD, followed by steady slowing of the dye removal until it achieves equilibrium in around 90 min. The main reason for its rapid removal from wastewater is the abundance of a significant proportion of unoccupied sites on the pristine sorbent surface at the initial stage of CV adsorption. These numbers of operational sites decrease as the adsorption of CV increases with time. Figure S1 depicts the impact of different initial dye concentrations of CV on the adsorption capacity (q$_e$). The graph shows that as the concentration of CV rises from 25 to 100 mg L^{-1}, the adsorbent increases the adsorption capacity. The greater the C$_o$ value (initial concentration), the greater the driving factor required to speed the adsorbate bulk transport from the solution to the interface of the adsorbent.
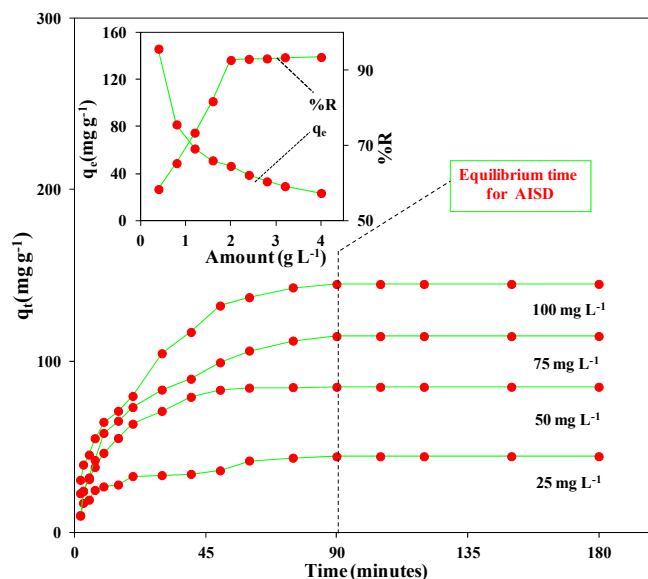
Figure 6. Effect of CV/AISD contact time on adsorption capacity for different initial dye concentrations at 303 K (inset—effect of adsorbent dose on adsorption capacity and percentage removal).

3.7.3. Effect of pH

The pH of the medium controls the degree of ionization and surface charge of the adsorbent, as well, and is therefore considered to be one of the most important controlling factors affecting the adsorption performance of the adsorbent. The impact of solution pH on CV dye sequestration by AISD was investigated in a wide range (2–13) for a typically chosen C_o of 100 mg L^{-1} (Figure 7). With a change in pH from 2 to 7, the q_e of the CV dye rose from 5.37 to 145.27 mg g^{-1} for AISD. A further increase in pH from 7 to 13 shows slight improvement in the adsorption capacity. The figure indicates that there is higher adsorption at a pH above 7. The increasing negative charge on the AISD surface due to the deprotonation of available functional groups has more potential to bind CV molecules at a higher pH. The adsorbent's point of zero charge (pH_{pzc}) is a remarkable way to understand the substantial influence of pH on adsorption. With the help of the solid-addition method, the pH_{pzc} of AISD was computed to be 6.3 (Figure 7 inset). Thus, at pH > 6.3, the surface AISD acquires a negative charge due to the deprotonation of the functional groups present on its surface and acts as an attractive site for the cationic CV molecules. In light of this, a pH value of 7.0 was chosen for further experiments.
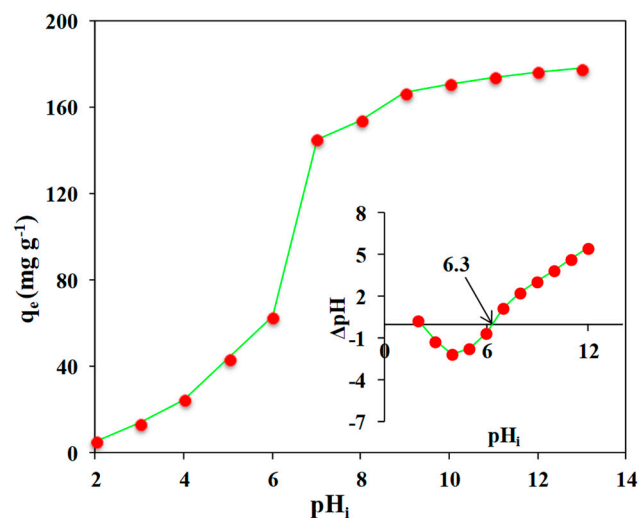

Figure 7. Effect of pH on the adsorption efficiency of CV dye (inset—pH_{pzc} of AISD).

3.8. Adsorption Kinetics

The time-dependent experiments were conducted and analyzed by employing various models, viz., pseudo-first-order (PFOR), pseudo-second-order (PSOR), Elovich (EVH), intraparticle diffusion (IDN), and liquid film diffusion (LDN). The linearized expressions for these models are listed in Table S1 [55]. The kinetic parameters as calculated for these models in the present case involving the adsorption of CV onto AISD are summarized in Table 1. Based on the R^2 values for different models, it may be concluded that PSOR best represents the adsorption of CV onto AISD. Thus the rate-limiting step may be chemical sorption or chemisorption involving valency forces through sharing or exchanging electrons between CV and AISD [65].

Table 1. Kinetic parameters for the adsorption of CV onto AISD (experimental conditions: adsorbent dose = 0.4 g L^{-1}, T = 303 K, pH = 7.0, and contact time = 90 min).

Kinetic Parameters	Initial Dye Concentration (C$_o$) in mg L^{-1}			
	25	50	75	100
Pseudo-first-order (PFOR)				
K$_1$ (min^{-1})	0.0417	0.0434	0.0818	0.0509
q$_{cal}$ (mg g^{-1})	32.593	102.9249	95.8035	145.5034
q$_{exp}$ (mg g^{-1})	44.273	84.811	114.388	144.745
R^2	0.8984	0.9689	0.9817	0.9660
Pseudo-second-order (PSOR)				
K$_2$ (g min^{-1} mg^{-1})	0.00248	0.00125	0.00063	0.00049
q$_{cal}$ (mg g^{-1})	46.948	90.909	125.000	158.730
q$_{exp}$ (mg g^{-1})	44.273	84.811	114.388	144.745
R^2	0.9969	0.9970	0.9979	0.9956
Interparticle diffusion model (IDN)				
K$_{id}$ (mg min$^{-\frac{1}{2}}$ g^{-1})	2.63536	5.7814	8.3504	10.645
C (constant)	16.103	26.513	26.476	32.861
R^2	0.8507	0.7603	0.8645	0.8728
Elovich (EVH)				
β (g mg^{-1})	0.1302	0.0572	0.0415	0.0330
α (mg g^{-1} min^{-1})	21.031	24.432	24.559	31.374
R^2	0.9684	0.9426	0.9762	0.9594
Liquid film diffusion (LDN)				
K$_{fd}$ (min^{-1})	0.0417	0.0998	0.0434	0.0618
D (constant)	−0.3063	−0.0275	−0.1056	−0.0914
R^2	0.8984	0.9929	0.9689	0.9710

The PSOR plot for AISD is given in Figure S2, indicating that the t/qt vs. t plots are uniform and have the best correlation coefficient value (R^2). Furthermore, the values of q$_e$ computed (q$_{cal}$) using this approach are more closely associated with the experimental q$_e$ (q$_{exp}$) values for AISD. In reality, the PSOR kinetics were already verified as the most fitting model concerning the elimination of CV by various adsorbent materials, as described in Table 2. The present findings are in a range comparable with previously published reported parameters.

The kinetics model may also assess the likelihood of CV adsorption via IDN onto the AISD. The possibility of IDN being the sole rate-limiting step can be indicated by the linear variation of q$_t$ vs. t$^{0.5}$ plot passing through origin with an intercept of 0 [66]. Because the q$_t$ versus t$^{0.5}$ intercept is non-zero (Table 1), we may assume that IDN is not the only rate-limiting step. To follow the LDN framework, the ln (1−F) vs. t plot should exhibit an intercept of 0. Table 1 shows that the LDN constant (D) values are between −0.3063 and

−0.0275 for AISD, implying that the liquid film diffusion model is unsuitable for CV dye adsorption.

Table 2. PSOR parameters for adsorption of CV onto different adsorbents.

Adsorbents	C_o (mg L^{-1})	M (g L^{-1})	K_2 (g min^{-1} mg^{-1})	q_e (mg g^{-1})	R^2	Reference
Sugercane bagasse	60	0.05	0.0172	59.27	0.9998	[67]
Rubber seed pericarp biomass/ sulfuric acid	50	0.06	0.444	87.60	0.9400	[68]
Charred rice husk (CRH)	50	0.025	0.00054	57.803	0.9974	[69]
Xanthated rice husk (XRH)	50	0.025	0.00060	71.428	0.9981	[69]
Bio-nanocomposite (Alg-Cst/Kal)	20	0.01	0.0204	29.24	0.9999	[70]
Tea waste/Fe$_3$O$_4$ magnetic composite	100	1.0	0.0023	111.11	0.9970	[71]
Coconut husk powder	100	0.1	0.000015	909.09	0.9948	[72]
Activated *Chromolaena odorata* biomass	50	15.0	0.000614	3.223	0.9999	[73]
Olive leaf powder	50	0.1	0.63	12.32	1.0000	[74]
Activated carbon of lemon wood (ACL)	10	1.25	0.009	8.545	0.9664	[75]
Magnetized activated carbon of lemon wood (ACL/Fe$_3$O$_4$)	10	1.25	0.0138	8.648	0.9730	[75]
Eucalyptus camdulensis biochar	20	0.5	0.011	38.55	0.8300	[76]
Rubber granulate and scrap polyurethane foam composite	50	0.1	0.0734	14.73	0.9984	[77]
Tectona grandis sawdust	50	2	0.0565	23.74	1.0000	[62]
Orange peel waste	50	2	0.007	22.730	0.9960	[78]
Magnetized orange peel waste	50	1	0.004	46.940	0.9870	[78]
Magnetized polypyrrole/chitosan	50	2	0.0024	23.732	0.995	[79]
Polyaniline/*Tectona grandis* sawdust	50	0.8	0.0128	59.64	1.0000	[80]
Cucumis sativus peels	50	5	0.20	9.71	0.9999	[81]
AISD	50	0.4	0.00125	90.909	0.9970	Present work

3.9. Adsorption Isotherm

The process governing the elimination of CV by AISD can also be better understood with the help of an adsorption isotherm as it helps us to establish a relationship within an adsorbate–adsorbent system. This relationship of the adsorbate–adsorbent system has been described using various isotherms frameworks. The Langmuir (LR), Freundlich (FH), and Temkin (TN) isotherm models are among them, and have been commonly used for the isotherm investigation. The LR model has relied on the idea that every unoccupied space can be singly adsorbed, having little connection between adsorbed molecules; it focuses on single-layer adsorption. Adsorption happens in a multilayered way with a complex composition of adsorption sites, which is explained under the FH isotherm model. The TN model states that adsorption is associated with the linear reduction in the heat of adsorption with the coverage of the adsorbent surface. The linear isotherm equations for all three models are listed in Table S1 [55].

The LR, FH, and TN isotherms were used to analyze the experimental results for isothermal studies of CV adsorption over AISD. Table 3 lists the variables obtained for various isotherm models at different temperatures as obtained in the present adsorbate–adsorbent system. The LR model was found to be the most suitable, indicating the mono-layer adsorption of CV onto AISD, as shown in Figure S3. The maximum single-layer adsorption capacity (q_m) was determined to be 270.27 mg g^{-1} after achieving the equilibrium time (90 min) at 303 K.

Table 3. Isotherm parameters for the adsorption of CV onto AISD (experimental conditions: adsorbent dose = 0.4 g L^{-1}, T = 303 K, pH = 7.0, and contact time = 90 min).

Isotherm Parameters	Temperature in K			
	303	**313**	**323**	**333**
Langmuir (LR)				
q_m (mg g^{-1})	270.27	285.72	322.58	370.37
K_L (L mg^{-1})	0.0270	0.0175	0.0170	0.0168
R^2	0.9978	0.9906	0.9930	0.9933
Freundlich (FH)				
N(constant)	1.502	1.122	1.1189	1.109
K_F (mg$^{1-1/n}$ L$^{1/n}$ g^{-1})	12.3073	2.5528	5.9097	6.60548
R^2	0.9882	0.9849	0.9888	0.9895
Temkin (TN)				
B (= RT b^{-1}; b (J mol^{-1}))	55.636	18.746	21.514	21.973
K_T (L g^{-1})	0.2936	0.3330	0.7382	0.8267
R^2	0.9897	0.9654	0.9694	0.9698

Furthermore, there is a non-dimensional factor $R_L = (\frac{1}{1+K_L C_o})$, whose magnitude specifies whether the operation is irreversible (0), linear (1), unfavorable (>1), or favorable (0–1). At 303 K, the determined R_L values for CV adsorption onto the AISD are 0.5967, 0.4253, 0.3303, and 0.2700 at C_o values of 25, 50, 75, and 100 mg L^{-1}, respectively. The fact that these numbers are in the 0–1 range verifies the favorability of an adsorption process. According to the relevant literature survey (Table 4), one can conclude that the Langmuir isotherm accurately represents the adsorption of CV by a wide range of adsorbents.

Table 4. LR isotherm parameters for adsorption of CV onto different adsorbents.

Adsorbents	M (g L^{-1})	K_L (L mg^{-1})	q_m (mg g^{-1})	R^2	References
Sugarcane bagasse	0.05	0.349	107.526	0.9900	[67]
Rubber seed pericarp biomass treated with sulfuric acid	0.025	0.510	567.600	0.9700	[68]
Tea waste/Fe$_3$O$_4$ magnetic composite	1.0	0.065	333.33	0.9890	[71]
Coconut husk powder	0.1	-	454.54	0.9980	[72]
Activated *Chromolaena odorata* biomass	15.0	40.0	142.85	0.9960	[73]
Olive leaf powder	0.1	0.042	133.33	0.9640	[74]
Activated carbon of lemon wood (ACL)	1.25	1.469	23.64	0.9704	[75]
Magnetized activated carbon of lemon wood (ACL/Fe$_3$O$_4$)	1.25	1.366	35.31	0.9826	[75]
Eucalyptus camdulensis biochar	0.5	26.14	54.64	0.9700	[76]
Rubber granulate (RG) and scrap polyurethane foam (PUF) composite	0.1	0.2284	20.92	0.9949	[77]
Tectona grandis sawdust	2	0.038	131.58	0.9980	[62]
Orange peel waste	2	0.210	138.88	0.9954	[78]
Magnetized orange peel waste	1	0.010	555.55	0.9912	[78]
Magnetized polypyrrole/chitosan	2	0.171	62.893	0.978	[79]
Polyaniline/*Tectona grandis* sawdust	0.8	0.148	263.2	0.9890	[80]
Cucumis sativus peels	5	0.03	149.25	0.9944	[81]
AISD	0.4	0.0270	270.27	0.9978	Present work

3.10. Adsorption Thermodynamics

This study helps us understand the feasibility of the adsorption process under the given set of conditions. Thermodynamic investigations accompanying the adsorption of CV onto AISD were carried out at different temperatures (303, 313, 323, and 333 K). The parameters, namely, enthalpy ($\Delta H°$), entropy ($\Delta S°$), and Gibb's free energy ($\Delta G°$) changes, were determined by employing the following mathematical formulae:

$$\Delta G° = - RT\ln K_c \qquad (4)$$

$$\ln K_c = \frac{-\Delta G°}{RT} = \frac{-\Delta H°}{RT} + \frac{\Delta S°}{R} \tag{5}$$

The distribution coefficient is represented by K_c, whereas the other variables have their conventional definitions. Table 5 lists the thermodynamic parameters as calculated from the slope and intercept of the $\ln K_c$ vs. T^{-1} plot (figure not shown). The adsorption process is associated with heat absorption and increased $\Delta S°$ at the adsorbent/adsorbate contact point. The increase in negative values of free energy changes with temperature suggests that the feasibility of adsorption increases with the temperature. Consequently, entropy plays a significant role in the adsorption process. Accordingly, the feasibility of adsorption is solitary due to the rise in entropy at the CV/AISD interface. Ultimately, the feasibility of the adsorption increases with an increase in temperature. An increase in entropy accompanying the adsorptive removal of CV by different adsorbents—namely, *Terminalia arjuna* sawdust [63], sugarcane bagasse [67], alginate/cysteine/kaolinite nanocomposite [70], rubber granulate/polyurethane foam composite [77], magnetized orange peel [78], polyaniline/*Tectona grandis* sawdust [80], *Punica granatum* seed [82], etc.—was also reported.

Table 5. Thermodynamics parameters for adsorption of CV onto AISD (experimental conditions: adsorbent dose = 0.4 g L^{-1}, T = 303 K, pH = 7.0, and contact time = 90 min).

Temperature (°C)	30	40	50	60
$-\Delta G°$ (kJ mol^{-1})	5.043	7.155	9.592	10.254
$\Delta H°$ (kJ mol^{-1})		50.0128		
$\Delta S°$ (J K^{-1} mol^{-1})		182.467		

3.11. Adsorption Mechanism

The scheme behind the adsorption pathway must be comprehended to understand the process better. However, before understanding the mechanism of adsorption, two key factors—the geometry and type of the adsorbate, and the adsorbent facet qualities, must be considered. The components present in AISD biomass are cellulose, hemicellulose, and lignin, along with smaller quantities of ash, moisture, volatile matter, etc. The former, as major constituents, contain –OH and –C=O groups, whereas the latter works as a gluing substrate to hold the cellulosic and hemicellulosic units together [83]. SEM/EDXS, TEM/SAED, and BET tests simply illustrated the highly porous surface morphology, small particle size on nano-scale, and good surface area. Since dye molecules in the nanometer scale range could readily permeate into the pores of AISD, this likely increased the binding of CV dye with AISD, and enhanced binding results in the effective removal of CV dye [83,84].

In AISD, the presence and participation of –OH, –C=O, and –NR$_2$ groups in binding CV molecules have been highlighted based on FTIR investigations. The increased adsorption of AISD suggests that dye adsorption is related to hydrogen bonding involving CV's hydroxyl groups and nitrogen atoms. A similar process was described on a NaOH-treated rice husk surface for the adsorption of CV [85]. Furthermore, the Coulomb force between negatively charged surface functional groups and the CV dye's positive charge core may significantly influence CV dye adsorption onto AISD. These interactions have been shown in a graphical format in Figure 8. Furthermore, at pH > pH$_{pzc}$, due to deprotonation of surface functional groups of adsorbents, it becomes strongly negatively charge, which with the positive core of CV shows enhanced binding, resulting in maximal CV dye absorption. When pH < pH$_{pzc}$, adsorption is much worse because of protonation of the adsorbent surface, which causes electrostatic repulsion. These forecasts are in line with those that have been made previously [86–89].
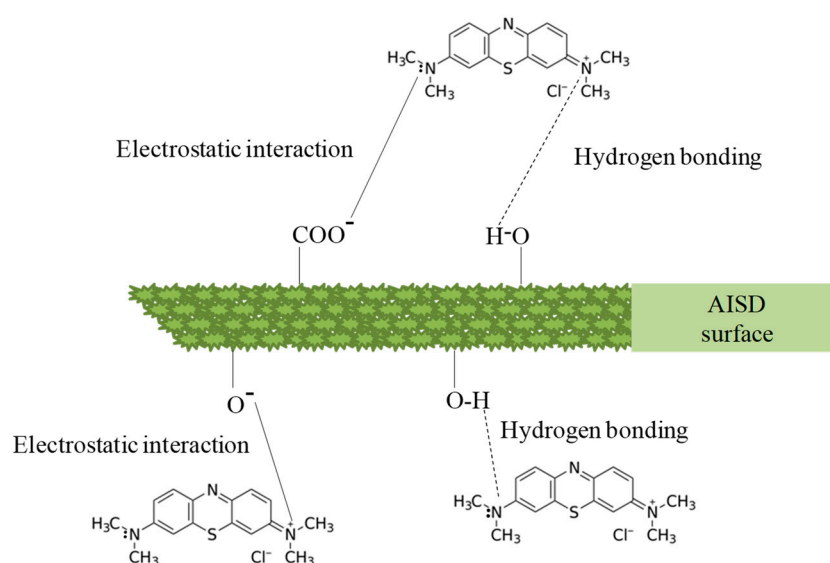
Figure 8. Proposed mechanism of adsorption of CV dye on AISD.

3.12. Desorption

Desorption tests with five desorbing agents, namely, NaOH, HCl, CH_3COOH, NaCl (0.1 M each), and DDDW, were performed to examine the better utility of the used adsorbent, and the resulting outcome is provided in Table S2. The best desorption was observed with 0.1M HCl.

The adsorbent should be reusable for several repeated adsorption-desorption cycles due to its better utility. In order to access the potential of the present adsorbent, four adsorption-desorption cycles were carried out with 0.1 M HCl solution, and the findings are illustrated in Figure S4. This figure points out that AISD can be effectively utilized for at least four repeated cycles to eliminate CV dye from an aqueous solution. A comparable finding was found when testing the NaOH-modified *Luffa aegyptica* peel in the adsorption of malachite green dye [55].

4. Conclusions

The current study evaluates the adsorptive performance of AISD in removing CV dye from wastewater. Different batch parameters altered the adsorption capacity of AISD, and it was found that equilibrium was reached in 90 min. The LR isotherm was observed to be best isotherm model with a maximal monolayer adsorption capacity of 270.27 mg g^{-1}. According to the kinetics research, the best model to represent the CV adsorption process onto AISD is the PSOR model, which represents the chemisorption type of adsorption, resulting in strong binding between CV and AISD. The thermodynamic analysis shows that CV adsorptions onto AISD is feasible, endothermic, and has positive $\Delta S°$ values. The maximal desorption of CV from AISD-CV for recycling AISD is exhibited by HCl (0.1M). The current study claims that this adsorbent is unique, effective, requires a minimal dose, has a high removal capacity, is economically cheap, and is likely recyclable for up to four cycles of adsorption/desorption for the sequestration of CV dye from wastewater. AISD has strong potential to be modified (chemically and magnetically) for further improvement of its adsorption capacity, separability, and recyclability. The AISD-based adsorbent must be exploited for persistent research on wastewater treatment containing a variety of contaminants, including dyes.

Supplementary Materials: The following supporting information can be downloaded at: https://www.mdpi.com/article/10.3390/suschem4010009/s1, Figure S1: The effects of initial dye concentration on the adsorption of CV onto the AISD, Figure S2: PSOR kinetic plots for the confiscation of CV dye onto AISD at varied starting dye concentrations Figure S3: LR adsorption isotherm for CV

adsorption onto AISD at 303 K, Figure S4: Reusability of AISD for four cycles, Table S1: Linear forms of kinetic, isothermal, and thermodynamic equations., Table S2: Desorption % of CV from AISD-CV.

References

1. Ahmed, T.; Imdad, S.; Yaldram, K.; Butt, N.M.; Pervez, A. Emerging nanotechnology-based methods for water purification: A review. *Desalin. Water Treat.* **2014**, *52*, 4089–4101. [CrossRef]
2. Jarup, L. Hazards of heavy metal contamination. *Br. Med. Bull.* **2003**, *68*, 167–182. [CrossRef] [PubMed]
3. Schwarzenbach, R.P.; Egli, T.; Hofstetter, T.B.; Von Gunten, U.; Wehrli, B. Global water pollution and human health. *Annu. Rev. Environ. Resour.* **2010**, *35*, 109–136. [CrossRef]
4. Jadhav, J.P.; Kalyani, D.C.; Telke, A.A.; Phugare, S.S.; Govindwar, S.P. Evaluation of the efficacy of a bacterial consortium for the removal of color, reduction of heavy metals, and toxicity from textile dye effluent. *Bioresour. Technol.* **2010**, *101*, 165–173. [CrossRef]
5. Kar, D.; Sur, P.; Mandai, S.K.; Saha, T.; Kole, R.K. Assessment of heavy metal pollution in surface water. *Int. J. Environ. Sci. Technol.* **2008**, *5*, 119–124. [CrossRef]
6. Prüss-Ustün, A.; Vickers, C.; Haefliger, P.; Bertollini, R. Knowns and unknowns on burden of disease due to chemicals: A systematic review. *Environ. Health* **2011**, *10*, 9. [CrossRef]
7. Tsuboy, M.S.; Angeli, J.P.F.; Mantovani, M.S.; Knasmüller, S.; Umbuzeiro, G.A.; Ribeiro, L.R. Genotoxic, mutagenic and cytotoxic effects of the commercial dye CI Disperse Blue 291 in the human hepatic cell line HepG2. *Toxicol. In Vitro* **2007**, *21*, 1650–1655. [CrossRef]
8. Barbosa, P.; Peters, T.M. The effects of vital dyes on living organisms with special reference to Methylene Blue and Neutral Red. *Histochem. J.* **1971**, *3*, 71–93. [CrossRef]
9. Kant, R. Textile dyeing industry an environmental hazard. *Nat. Sci.* **2012**, *04*, 22–26. [CrossRef]
10. Verma, A.K.; Dash, R.R.; Bhunia, P. A review on chemical coagulation/flocculation technologies for removal of colour from textile wastewaters. *J. Environ. Manag.* **2012**, *93*, 154–168. [CrossRef]
11. Cassano, A.; Molinari, R.; Romano, M.; Drioli, E. Treatment of aqueous effluents of the leather industry by membrane processes. *J. Membr. Sci.* **2001**, *181*, 111–126. [CrossRef]
12. Crini, G. Non-conventional low-cost adsorbents for dye removal: A review. *Bioresour. Technol.* **2006**, *97*, 1061–1085. [CrossRef]
13. Forgacs, E.; Cserháti, T.; Oros, G. Removal of synthetic dyes from wastewaters: A review. *Environ. Int.* **2004**, *30*, 953–971. [CrossRef]
14. Mittal, A.; Mittal, J.; Malviya, A.; Kaur, D.; Gupta, V.K. Adsorption of hazardous dye crystal violet from wastewater by waste materials. *J. Colloid Interface Sci.* **2010**, *343*, 463–473. [CrossRef] [PubMed]
15. Brown, D. Effects of colorants in the aquatic environment. *Ecotoxicol. Environ. Saf.* **1987**, *13*, 139–147. [CrossRef] [PubMed]
16. Deshannavar, U.B.B.; Ratnamala, G.M.M.; Kalburgi, P.B.B.; El-Harbawi, M.; Agarwal, A.; Shet, M.; Teli, M.; Bhandare, P. Optimization, Kinetic and Equilibrium Studies of Disperse Yellow 22 Dye Removal from Aqueous Solutions Using Malaysian Teak Wood Sawdust as Adsorbent. *Indian Chem. Eng.* **2016**, *58*, 12–28. [CrossRef]
17. Mani, S.; Bharagava, R.N. Exposure to Crystal Violet, Its Toxic, Genotoxic and Carcinogenic Effects on Environment and Its Degradation and Detoxification for Environmental Safety. In *Reviews of Environmental Contamination and Toxicology*; Springer: Cham, Switzerland, 2016; pp. 71–104.
18. Wu, J.; Eiteman, M.A.; Law, S.E. Evaluation of Membrane Filtration and Ozonation Processes for Treatment of Reactive-Dye Wastewater. *J. Environ. Eng.* **1998**, *124*, 272–277. [CrossRef]
19. Soltani, A.; Faramarzi, M.; Mousavi Parsa, S.A. A review on adsorbent parameters for removal of dye products from industrial wastewater. *Water Qual. Res. J.* **2021**, *56*, 181–193. [CrossRef]

20. Rezakazemi, M.; Khajeh, A.; Mesbah, M. Membrane filtration of wastewater from gas and oil production. *Environ. Chem. Lett.* **2018**, *16*, 367–388. [CrossRef]

21. Malkoske, T.A.; Bérubé, P.R.; Andrews, R.C. Coagulation/flocculation prior to low pressure membranes in drinking water treatment: A review. *Environ. Sci. Water Res. Technol.* **2020**, *6*, 2993–3023. [CrossRef]

22. Hassan, M.M.; Carr, C.M. A critical review on recent advancements of the removal of reactive dyes from dyehouse effluent by ion-exchange adsorbents. *Chemosphere* **2018**, *209*, 201–219. [CrossRef] [PubMed]

23. Bashir, A.; Malik, L.A.; Ahad, S.; Manzoor, T.; Bhat, M.A.; Dar, G.N.; Pandith, A.H. Removal of heavy metal ions from aqueous system by ion-exchange and biosorption methods. *Environ. Chem. Lett.* **2019**, *17*, 729–754. [CrossRef]

24. Robinson, T.; McMullan, G.; Marchant, R.; Nigam, P. Remediation of dyes in textile effluent: A critical review on current treatment technologies with a proposed alternative. *Bioresour. Technol.* **2001**, *77*, 247–255. [CrossRef] [PubMed]

25. Dos Santos, A.B.; Cervantes, F.J.; van Lier, J.B. Review paper on current technologies for decolourisation of textile wastewaters: Perspectives for anaerobic biotechnology. *Bioresour. Technol.* **2007**, *98*, 2369–2385. [CrossRef]

26. Korngold, E.; Kock, K.; Strathmann, H. Electrodialysis in advanced waste water treatment. *Desalination* **1977**, *24*, 129–139. [CrossRef]

27. Aragaw, T.A.; Bogale, F.M. Biomass-Based Adsorbents for Removal of Dyes From Wastewater: A Review. *Front. Environ. Sci.* **2021**, *9*, 764958. [CrossRef]

28. Al-Amshawee, S.; Yunus, M.Y.B.M.; Azoddein, A.A.M.; Hassell, D.G.; Dakhil, I.H.; Hasan, H.A. Electrodialysis desalination for water and wastewater: A review. *Chem. Eng. J.* **2020**, *380*, 122231. [CrossRef]

29. Mohammadi, T.; Moheb, A.; Sadrzadeh, M.; Razmi, A. Modeling of metal ion removal from wastewater by electrodialysis. *Sep. Purif. Technol.* **2005**, *41*, 73–82. [CrossRef]

30. Amuda, O.; Amoo, I. Coagulation/flocculation process and sludge conditioning in beverage industrial wastewater treatment. *J. Hazard. Mater.* **2007**, *141*, 778–783. [CrossRef]

31. Bahnemann, D. Photocatalytic water treatment: Solar energy applications. *Sol. Energy* **2004**, *77*, 445–459. [CrossRef]

32. Houas, A.; Lachheb, H.; Ksibi, M.; Elaloui, E.; Guillard, C.; Herrmann, J.M. Photocatalytic degradation pathway of methylene blue in water. *Appl. Catal. B Environ.* **2001**, *31*, 145–157. [CrossRef]

33. Chakraborty, S.; Purkait, M.K.; DasGupta, S.; De, S.; Basu, J.K. Nanofiltration of textile plant effluent for color removal and reduction in COD. *Sep. Purif. Technol.* **2003**, *31*, 141–151. [CrossRef]

34. Al-Rashdi, B.A.M.; Johnson, D.J.; Hilal, N. Removal of heavy metal ions by nanofiltration. *Desalination* **2013**, *315*, 2–17. [CrossRef]

35. Chen, X.; Chen, G.; Yue, P.L. Novel Electrode System for Electroflotation of Wastewater. *Environ. Sci. Technol.* **2002**, *36*, 778–783. [CrossRef]

36. De Oliveira da Mota, I.; de Castro, J.A.; de Góes Casqueira, R.; de Oliveira Junior, A.G. Study of electroflotation method for treatment of wastewater from washing soil contaminated by heavy metals. *J. Mater. Res. Technol.* **2015**, *4*, 109–113. [CrossRef]

37. Kolesnikov, V.A.; Il'in, V.I.; Kolesnikov, A.V. Electroflotation in Wastewater Treatment from Oil Products, Dyes, Surfactants, Ligands, and Biological Pollutants: A Review. *Theor. Found. Chem. Eng.* **2019**, *53*, 251–273. [CrossRef]

38. Qamruzzaman; Nasar, A. Kinetics of metribuzin degradation by colloidal manganese dioxide in absence and presence of surfactants. *Chem. Pap.* **2014**, *68*, 65–73. [CrossRef]

39. Qamruzzaman; Nasar, A. Treatment of acetamiprid insecticide from artificially contaminated water by colloidal manganese dioxide in the absence and presence of surfactants. *RSC Adv.* **2014**, *4*, 62844–62850. [CrossRef]

40. Qamruzzaman; Nasar, A. Degradation of acephate by colloidal manganese dioxide in the absence and presence of surfactants. *Desalin. Water Treat.* **2015**, *55*, 2155–2164. [CrossRef]

41. Greenlee, L.F.; Lawler, D.F.; Freeman, B.D.; Marrot, B.; Moulin, P. Reverse osmosis desalination: Water sources, technology, and today's challenges. *Water Res.* **2009**, *43*, 2317–2348. [CrossRef]

42. Qasim, M.; Badrelzaman, M.; Darwish, N.N.; Darwish, N.A.; Hilal, N. Reverse osmosis desalination: A state-of-the-art review. *Desalination* **2019**, *459*, 59–104. [CrossRef]

43. Li, X.; Hasson, D.; Semiat, R.; Shemer, H. Intermediate concentrate demineralization techniques for enhanced brackish water reverse osmosis water recovery—A review. *Desalination* **2019**, *466*, 24–35. [CrossRef]

44. Thaçi, B.; Gashi, S. Reverse Osmosis Removal of Heavy Metals from Wastewater Effluents Using Biowaste Materials Pretreatment. *Pol. J. Environ. Stud.* **2018**, *28*, 337–341. [CrossRef]

45. Lin, S.H.; Lin, C.M. Treatment of textile waste effluents by ozonation and chemical coagulation. *Water Res.* **1993**, *27*, 1743–1748. [CrossRef]

46. Khamparia, S.; Jaspal, D.K. Adsorption in combination with ozonation for the treatment of textile waste water: A critical review. *Front. Environ. Sci. Eng.* **2017**, *11*, 8. [CrossRef]

47. Wang, J.; Chen, H. Catalytic ozonation for water and wastewater treatment: Recent advances and perspective. *Sci. Total Environ.* **2020**, *704*, 135249. [CrossRef] [PubMed]

48. Panizza, M. Electrochemical treatment of wastewater containing polyaromatic organic pollutants. *Water Res.* **2000**, *34*, 2601–2605. [CrossRef]

49. Nidheesh, P.V.; Zhou, M.; Oturan, M.A. An overview on the removal of synthetic dyes from water by electrochemical advanced oxidation processes. *Chemosphere* **2018**, *197*, 210–227. [CrossRef] [PubMed]

50. Singh, H.; Chauhan, G.; Jain, A.K.; Sharma, S.K. Adsorptive potential of agricultural wastes for removal of dyes from aqueous solutions. *J. Environ. Chem. Eng.* **2017**, *5*, 122–135. [CrossRef]

51. Bhatnagar, A.; Sillanpää, M.; Witek-Krowiak, A. Agricultural waste peels as versatile biomass for water purification—A review. *Chem. Eng. J.* **2015**, *270*, 244–271. [CrossRef]

52. Nasar, A. Utilization of tea wastes for the removal of toxic dyes from polluted water—A review. *Biomass Convers. Biorefinery* **2021**, *13*, 399–1415. [CrossRef]

53. Khattri, S.D.; Singh, M.K. Removal of malachite green from dye wastewater using neem sawdust by adsorption. *J. Hazard. Mater.* **2009**, *167*, 1089–1094. [CrossRef]

54. Bhattacharyya, K.G.; Sharma, A. Kinetics and thermodynamics of Methylene Blue adsorption on Neem (Azadirachta indica) leaf powder. *Dye. Pigment.* **2005**, *65*, 51–59. [CrossRef]

55. Mashkoor, F.; Nasar, A. Preparation, characterization and adsorption studies of the chemically modified Luffa aegyptica peel as a potential adsorbent for the removal of malachite green from aqueous solution. *J. Mol. Liq.* **2019**, *274*, 315–327. [CrossRef]

56. Thommes, M.; Kaneko, K.; Neimark, A.V.; Olivier, J.P.; Rodriguez-Reinoso, F.; Rouquerol, J.; Sing, K.S.W. Physisorption of gases, with special reference to the evaluation of surface area and pore size distribution (IUPAC Technical Report). *Pure Appl. Chem.* **2015**, *87*, 1051–1069. [CrossRef]

57. Eskandari, M.; García, C.A.; Buceta, D.; Malekfar, R.; Taboada, P. NiCo$_2$O$_4$/MWCNT/PANI coral-like nanostructured composite for electrochemical energy-storage applications. *J. Electroanal. Chem.* **2019**, *851*, 113481. [CrossRef]

58. Basu, M.; Guha, A.K.; Ray, L. Adsorption of Lead on Cucumber Peel. *J. Clean. Prod.* **2017**, *151*, 603–615. [CrossRef]

59. Shaaban, A.; Se, S.-M.; Mitan, N.M.M.; Dimin, M.F. Characterization of Biochar Derived from Rubber Wood Sawdust through Slow Pyrolysis on Surface Porosities and Functional Groups. *Procedia Eng.* **2013**, *68*, 365–371. [CrossRef]

60. Wang, Z.; Cao, J.; Wang, J. Pyrolytic characteristics of pine wood in a slowly heating and gas sweeping fixed-bed reactor. *J. Anal. Appl. Pyrolysis* **2009**, *84*, 179–184. [CrossRef]

61. Jiang, Z.-H.H.; Yang, Z.; So, C.-L.L.; Hse, C.-Y.Y. Rapid prediction of wood crystallinity in Pinus elliotii plantation wood by near-infrared spectroscopy. *J. Wood Sci.* **2007**, *53*, 449–453. [CrossRef]

62. Mashkoor, F.; Nasar, A.; Inamuddin; Asiri, A.M. Exploring the Reusability of Synthetically Contaminated Wastewater Containing Crystal Violet Dye using Tectona grandis Sawdust as a Very Low-Cost Adsorbent. *Sci. Rep.* **2018**, *8*, 8314. [CrossRef] [PubMed]

63. Shakoor, S.; Nasar, A. Adsorptive decontamination of synthetic wastewater containing crystal violet dye by employing Terminalia arjuna sawdust waste. *Groundw. Sustain. Dev.* **2018**, *7*, 30–38. [CrossRef]

64. Yang, H.; Yan, R.; Chen, H.; Lee, D.H.; Zheng, C. Characteristics of hemicellulose, cellulose and lignin pyrolysis. *Fuel* **2007**, *86*, 1781–1788. [CrossRef]

65. Ho, Y.S.; McKay, G. Pseudo-second order model for sorption processes. *Process Biochem.* **1999**, *34*, 451–465. [CrossRef]

66. Doğan, M.; Abak, H.; Alkan, M. Adsorption of methylene blue onto hazelnut shell: Kinetics, mechanism and activation parameters. *J. Hazard. Mater.* **2009**, *164*, 172–181. [CrossRef]

67. Omer, A.S.; Naeem, G.A.; Abd-Elhamid, A.; Farahat, O.O.; El-Bardan, A.A.; Soliman, H.M.; Nayl, A. Adsorption of crystal violet and methylene blue dyes using a cellulose-based adsorbent from sugercane bagasse: Characterization, kinetic and isotherm studies. *J. Mater. Res. Technol.* **2022**, *19*, 3241–3254. [CrossRef]

68. Uddin, M.K.; Abd Malek, N.N.; Jawad, A.H.; Sabar, S. Pyrolysis of rubber seed pericarp biomass treated with sulfuric acid for the adsorption of crystal violet and methylene green dyes: An optimized process. *Int. J. Phytoremediat.* **2023**, *25*, 393–402. [CrossRef]

69. Homagai, P.L.; Poudel, R.; Poudel, S.; Bhattarai, A. Adsorption and removal of crystal violet dye from aqueous solution by modified rice husk. *Heliyon* **2022**, *8*, e09261. [CrossRef]

70. Mittal, J.; Ahmad, R.; Ejaz, M.O.; Mariyam, A.; Mittal, A. A novel, eco-friendly bio-nanocomposite (Alg-Cst/Kal) for the adsorptive removal of crystal violet dye from its aqueous solutions. *Int. J. Phytoremediat.* **2022**, *24*, 796–807. [CrossRef]

71. Kumbhar, P.; Narale, D.; Bhosale, R.; Jambhale, C.; Kim, J.-H.H.; Kolekar, S. Synthesis of tea waste/Fe3O4 magnetic composite (TWMC) for efficient adsorption of crystal violet dye: Isotherm, kinetic and thermodynamic studies. *J. Environ. Chem. Eng.* **2022**, *10*, 107893. [CrossRef]

72. Sultana, S.; Islam, K.; Hasan, M.A.; Khan, H.M.J.; Khan, M.A.R.; Deb, A.; Al Raihan, M.; Rahman, M.W. Adsorption of crystal violet dye by coconut husk powder: Isotherm, kinetics and thermodynamics perspectives. *Environ. Nanotechnol. Monit. Manag.* **2022**, *17*, 100651. [CrossRef]

73. Soosai, M.R.; Moorthy, I.M.G.; Varalakshmi, P.; Syed, A.; Elgorban, A.M.; Rigby, S.P.; Natesan, S.; Gunaseelan, S.; Joshya, Y.C.; Baskar, R.; et al. Use of activated Chromolaena odorata biomass for the removal of crystal violet from aqueous solution: Kinetic, equilibrium, and thermodynamic study. *Environ. Sci. Pollut. Res.* **2023**, *30*, 14265–14283. [CrossRef]

74. Elsherif, K.M.; El-Dali, A.; Alkarewi, A.A.; Ewlad-ahmed, A.M.; Treban, A. Adsorption of crystal violet dye onto olive leaves powder: Equilibrium and kinetic studies. *Chem. Int.* **2021**, *7*, 79–89.

75. Foroutan, R.; Peighambardoust, S.H.J.; Peighambardoust, S.H.J.; Pateiro, M.; Lorenzo, J.M. Adsorption of Crystal Violet Dye Using Activated Carbon of Lemon Wood and Activated Carbon/Fe$_3$O$_4$ Magnetic Nanocomposite from Aqueous Solutions: A Kinetic, Equilibrium and Thermodynamic Study. *Molecules* **2021**, *26*, 2241. [CrossRef] [PubMed]

76. Amin, M.T.; Alazba, A.A.; Shafiq, M. Successful Application of Eucalyptus Camdulensis Biochar in the Batch Adsorption of Crystal Violet and Methylene Blue Dyes from Aqueous Solution. *Sustainability* **2021**, *13*, 3600. [CrossRef]

77. Sulyman, M.; Kucinska-Lipka, J.; Sienkiewicz, M.; Gierak, A. Development, characterization and evaluation of composite adsorbent for the adsorption of crystal violet from aqueous solution: Isotherm, kinetics, and thermodynamic studies. *Arab. J. Chem.* **2021**, *14*, 103115. [CrossRef]

78. Ahmed, M.; Mashkoor, F.; Nasar, A. Development, characterization, and utilization of magnetized orange peel waste as a novel adsorbent for the confiscation of crystal violet dye from aqueous solution. *Groundw. Sustain. Dev.* **2020**, *10*, 100322. [CrossRef]

79. Mashkoor, F.; Nasar, A. Facile synthesis of polypyrrole decorated chitosan-based magsorbent: Characterizations, performance, and applications in removing cationic and anionic dyes from aqueous medium. *Int. J. Biol. Macromol.* **2020**, *161*, 88–100. [CrossRef]

80. Mashkoor, F.; Nasar, A. Polyaniline/Tectona grandis sawdust: A novel composite for efficient decontamination of synthetically polluted water containing crystal violet dye. *Groundw. Sustain. Dev.* **2019**, *8*, 390–401. [CrossRef]

81. Shakoor, S.; Nasar, A. Utilization of *Cucumis Sativus* Peel as an Eco-Friendly Biosorbent for the Confiscation of Crystal Violet Dye from Artificially Contaminated Wastewater. *Anal. Chem. Lett.* **2019**, *9*, 1–19. [CrossRef]

82. Uddin, M.K.; Nasar, A. Decolorization of Basic Dyes Solution by Utilizing Fruit Seed Powder. *KSCE J. Civ. Eng.* **2020**, *24*, 345–355. [CrossRef]

83. Chowdhury, S.; Mishra, R.; Saha, P.; Kushwaha, P. Adsorption thermodynamics, kinetics and isosteric heat of adsorption of malachite green onto chemically modified rice husk. *Desalination* **2011**, *265*, 159–168. [CrossRef]

84. Valadez-Gonzalez, A.; Cervantes-Uc, J.; Olayo, R.; Herrera-Franco, P. Effect of fiber surface treatment on the fiber–matrix bond strength of natural fiber reinforced composites. *Compos. Part B* **1999**, *309*, 20. [CrossRef]

85. Chakraborty, S.; Chowdhury, S.; Das Saha, P. Adsorption of crystal violet from aqueous solution onto NaOH-modified rice husk. *Carbohydr. Polym.* **2011**, *86*, 1533–1541. [CrossRef]

86. Leng, L.; Yuan, X.; Zeng, G.; Shao, J.; Chen, X.; Wu, Z.; Wang, H.; Peng, X. Surface characterization of rice husk bio-char produced by liquefaction and application for cationic dye (Malachite green) adsorption. *Fuel* **2015**, *155*, 77–85. [CrossRef]

87. Leng, L.; Yuan, X.; Huang, H.; Wang, H.; Wu, Z.; Fu, L.; Peng, X.; Chen, X.; Zeng, G. Characterization and application of bio-chars from liquefaction of microalgae, lignocellulosic biomass and sewage sludge. *Fuel Process. Technol.* **2015**, *129*, 8–14. [CrossRef]

88. Leng, L.; Yuan, X.; Huang, H.; Shao, J.; Wang, H.; Chen, X.; Zeng, G. Bio-char derived from sewage sludge by liquefaction: Characterization and application for dye adsorption. *Appl. Surf. Sci.* **2015**, *346*, 223–231. [CrossRef]

89. Wang, H.; Yuan, X.; Zeng, G.; Leng, L.; Peng, X.; Liao, K.; Peng, L.; Xiao, Z. Removal of malachite green dye from wastewater by different organic acid-modified natural adsorbent: Kinetics, equilibriums, mechanisms, practical application, and disposal of dye-loaded adsorbent. *Environ. Sci. Pollut. Res.* **2014**, *21*, 11552–11564. [CrossRef]